*minerals*

MDPI

*Article*

# Investigation of the Effect of Fracturing Fluids on Shale Pore Structure by Nuclear Magnetic Resonance

**Xiulan Zhu [1,2,3,4], Zhiguo Wang [5,6], Yang You [7], Chuang Zhang [8], Hui Gao [1,3,4,*], Nan Zhang [9], Teng Li [1,3,4], Chen Wang [1,3,4] and Zhilin Cheng [1,3,4]**

1 School of Petroleum Engineering, Xi'an Shiyou University, Xi'an 710065, China; zhuxltj@126.com (X.Z.); liteng2052@163.com (T.L.); cwangxsyu@163.com (C.W.); zhilin_cheng1992@163.com (Z.C.)
2 School of Petrochemical Engineering, Longdong University, Qingyang 745000, China
3 Engineering Research Center of Development and Management for Low to Ultra-Low Permeability Oil & Gas Reservoirs in West China, Ministry of Education, Xi'an 710065, China
4 Xi'an Key Laboratory of Tight Oil (Shale Oil) Development, Xi'an 710065, China
5 Oil and Gas Technology Institute of Changqing Oilfield Company, PetroChina, Xi'an 710018, China; wzguo_cq@petrochina.com.cn
6 National Engineering Laboratory for Exploration and Development of Low-Permeability Oil & Gas Fields, Xi'an 710018, China
7 Natural Gas Research Institute, Shaanxi Yanchang Petroleum (Group) Co., Ltd., Xi'an 710075, China
8 Zhidan Oil Production Plant of Yanchang Oilfield Co., Ltd., Yan'an 717500, China
9 Department of Electrical Engineering and Computer Science, University of Stavanger, 4036 Stavanger, Norway; nan.zhang@uis.no
* Correspondence: gh@xsyu.edu.cn

**Abstract:** Hydraulic fracturing technology significantly enhances the productivity of shale oil and gas reservoirs. Nonetheless, the infiltration of fracturing fluid into shale formations can detrimentally affect the microscopic pore structure, thereby impairing the efficacy of hydraulic stimulation. In this study, nuclear magnetic resonance (NMR) technology was utilized to conduct high-pressure soaking tests on shale specimens treated with EM30$^+$ + guar gum mixed water and CNI nano variable-viscosity slickwater, where various concentrations of a drag reducer were utilized. Additionally, the differences in porosity, permeability, mineral composition, and iron ion concentration before and after the measurements were compared, which were used to analyze the influence on the shale's microscopic pore structure. It features a reduction in the total pore volume after the interaction with the fracturing fluid, with the pore-throat damage degree, porosity damage degree, and permeability damage degree ranging from 0.63% to 5.62%, 1.51% to 6.84%, and 4.17% to 19.61%, respectively. Notably, EM30$^+$ + guar gum mixed water exhibits heightened adsorption retention, alkaline dissolution, and precipitation compared to CNI nano variable-viscosity slickwater, rendering it more deleterious to shale. Moreover, higher concentrations of drag reducers, such as EM30$^+$ or CNI-B, predominantly result in damage to the shale's micropores. Shale compositions characterized by lower content of quartz and elevated proportions of clay minerals and iron-bearing minerals showcase augmented mineral dissolution and precipitation, consequently intensifying the shale damage. The hydration expansion of mixed-layer illite/smectite profoundly diminishes the core permeability. Consequently, the mechanisms underpinning the damage inflicted on shale's microscopic pore structure primarily involve fracturing fluid adsorption and retention, mineral dissolution, and precipitation, such as clay minerals and iron-containing minerals.

**Keywords:** NMR; pore structure; fracturing fluid type; mineral dissolution and precipitation; iron-containing minerals; damage characteristics



**Citation:** Zhu, X.; Wang, Z.; You, Y.; Zhang, C.; Gao, H.; Zhang, N.; Li, T.; Wang, C.; Cheng, Z. Investigation of the Effect of Fracturing Fluids on Shale Pore Structure by Nuclear Magnetic Resonance. *Minerals* **2023**, *13*, 1405. https://doi.org/10.3390/min13111405

Academic Editor: Gianvito Scaringi

Received: 17 September 2023
Revised: 25 October 2023
Accepted: 30 October 2023
Published: 1 November 2023



## 1. Introduction

Shale oil and gas, as the most potential strategic replacement resources, are also hot spots for exploration and development in the global oil field in recent years [1–5]. Hydraulic

fracturing technology has become an essential method to develop shale oil and gas effectively [6–8]. Hydraulic fracturing forms artificial fractures in the shale, accompanied by the intrusion of fracturing fluids into the shale matrix. The physicochemical interactions occur between the fracturing fluid and shale, such as water sensitivity, water locking, blockage of solid residual particles, adsorption and retention of fracturing fluid, mineral dissolution, and precipitation [9–14]. In particular, the original microscopic pore structure is altered due to the retention of the fracturing fluids in the shale reservoirs, thereby restricting the stimulation effect. Additionally, the permeability damage degree of shale is significantly higher than that of tight sandstone during the fracturing procedures [15]. It is a key issue that the formation damage is induced by fracturing fluid for the effective development of shale oil and gas reservoirs [16]. Therefore, the damage characteristics of shale's microscopic pore structure are evaluated, its microscopic damage mechanism is revealed, and the optimizing performance of the fracturing fluid and improvement in the stimulation effect of hydraulic fracturing are discussed.

The former studies reported the reservoir damage induced by fracturing liquid [17–21]. Shale with a high content of clay minerals is facilely hydrated, and the hydration damage is aggravated due to the bedding structure and clay mineral orientation [22–25]. Bazin et al. [26] reported that water-based fracturing fluids lead to clay mineral expansion and particle migration, leading to a sharp decline in core permeability. Clay swelling inhibitors can be added to fracturing fluids to mitigate clay swelling, such as new gemini surfactants, dicationic surfactants, and imidazolium-based ionic liquids [27–29]. Furthermore, the fracturing fluid molecules would be adsorbed on the rock surface, particle edges, and rock bedding planes through hydrogen bonding, and entangled with each other to block pores [30]. Complex chemical reactions between fracturing fluids and shale minerals induce mineral dissolution, such as silicate minerals, carbonate minerals, iron-containing minerals, the release and migration of chemical components, and the formation of new mineral precipitation, resulting in changes in permeability and porosity [31–34]. Lu et al. [35] proposed that the dissolution of shale minerals caused an increase in the pore volume, while ion precipitation and chemical agent adsorption led to a decrease in the pore volume. Qi et al. [36] found that a decrease in the effective pore volume and an increase in the number of pores occurred at the early stage of fluid incursion. The pore size of larger intergranular pores were enlarged in the high-pressure invasion process. Fractures and small dissolved pores were the main areas where fracturing fluid stagnated. The guar gum fracturing fluid and slick water fracturing fluid were dominantly utilized in the unconventional reservoir fracturing, while the differences of formulations and properties of fracturing fluids would lead to a discrepancy in the microscopic damage of the reservoir [37]. Sun et al. [38] concluded that the cross-linked gel promoted the precipitation of carbonate minerals, whereas the slick water induced carbonate minerals to form the dissolute pores. Cheng et al. [39] pointed out that guanidine gum gelout formed flocculent sediments in pores, and slickwater eroded the gaps at the pore edges. At present, multiple testing techniques are used to characterize the retained morphology of the fracturing fluid, microscopic pore structure, and variations in mineral components [31,36,40,41], including scanning electron microscope (SEM), atomic force microscope (AFM), X-ray diffraction (XRD), high-pressure mercury intrusion (HPMI), low-pressure nitrogen adsorption (LPNA), NMR, and Computed Tomography (CT) scanning, etc. Li et al. [41] comprehensively and quantitatively evaluated the damage degree of fracturing fluid through displacement experiments and NMR. NMR is an effective method to represent the micro-pore structure of rocks on a full scale. It is also used to discern the characteristics of pore types at different scales, and it would not alter the mineral, pore structure, and fluid occurrence [42,43].

The damaging effect of the fracturing fluid macroscopically manifested as the reduction of core porosity and permeability. However, the nanoscale pore structure of shale is extremely complicated, and the damage characteristics inflicted by fracturing fluids on the shale's microscopic pore structure are still unclear. Meanwhile, few studies have focused on the formation damage originated by iron-bearing minerals. In this study, two

different types of fracturing fluids were selected, $EM30^+$ + guar gum mixed water and CNI nano variable-viscosity slickwater, respectively. Under high-temperature and -pressure conditions, shale soaking tests were performed to obtain the NMR $T_2$ spectrum of the shales saturated with formation water before and after the experiment. The damage characteristics of the shale pore at different scales were quantitatively characterized. Moreover, relevant parameters, such as porosity, permeability, mineral composition, and iron ion concentration were obtained to discern the discrepancy, which were used to evaluated the damage on the microscopic pore structure. Finally, the damage mechanism of the fracturing fluid on shale's microscopic pore structure is elaborated. The novelty of this work is to compare the difference in the effects of shale pore structure by $EM30^+$ + guar gum mixed water and CNI nano variable-viscosity slickwater and to clarify the microscopic damage of shale by iron-containing minerals or iron ions. These findings provide technical support for fracturing simulation and production enhancement in shale oil and gas reservoirs.

## 2. Materials and Methods

### *2.1. Experimental Materials*

The experimental samples were taken from the laminar shale of the Chang $7_3$ Member of the Triassic Yanchang Formation in the Ordos Basin, China. The mudstone and fine siltstone feature as thin interbedded layers in the shale. The laminar shale of the Chang $7_3$ Member exhibits extremely low porosity and permeability and well-developed nanoscale pore-throat fractures. The basic information of experimental samples is shown in Table 1.

**Table 1.** Basic information of experimental samples.

| Core No. | Porosity (%) | Permeability ($10^{-3}$ μm$^2$) | Fracturing Fluid Types and Drag Reducer Concentrations |
|---|---|---|---|
| A1-2 | 4.49 | 0.0054 | $EM30^+$ + guar gum mixed water (0.15% $EM30^+$ drag reducer) |
| A2-2 | 4.24 | 0.0051 | $EM30^+$ + guar gum mixed water (0.35% $EM30^+$ drag reducer) |
| B1-2 | 3.97 | 0.0048 | CNI nano variable-viscosity slickwater (0.06% CNI-B drag reducer) |
| B2-2 | 4.11 | 0.0053 | CNI nano variable-viscosity slickwater (0.08% CNI-B drag reducer) |

As for the shale high-pressure soaking test, the formation water was prepared with a salinity of 49,300 mg/L $CaCl_2$. The fracturing fluid filtrates were applied after breaking and static filtration as the displacement agent; therefore, the harmful effects of solid phase residues and particles could be ignored. The fracturing fluid types were $EM30^+$ + guar gum mixed water and CNI nano variable-viscosity slickwater, respectively. The concentrations of $EM30^+$ drag reducer were 0.15% and 0.35% in $EM30^+$ + guar gum mixed water, respectively. The pH value was set between 9 and 10. The hydroxyl groups of guar gum molecules formed strong multiple hydrogen bond forces with the oxygen-containing groups on the rock surface. The adsorption and retention of fracturing fluid was enhanced. The concentrations of CNI-B drag reducer were 0.06% and 0.08%, respectively. Moreover, the pH value of CNI nano variable-viscosity slickwater was 7. CNI-B drag reducer was a polyacrylamide polymer, whose hydrophilic group generated a chemical bond with the oxygen-containing group in shale, adsorbing and sticking on the micro-fracture wall and matrix pores [44].

### *2.2. Shale High-Pressure Soaking Test*

The equipment for the NMR-based shale high-pressure soaking test mainly includes a PQ001 type NMR analyzer, an NM-V type vacuum pressurization and saturation device, a ZR-3 type piston intermediate container, a high-pressure pump, and a constant temperature heating device. The inner diameter of the probe of NMR analyzer is 2.86 cm, which is

suitable for core samples with a diameter of 2.54 cm and a height of no less than 2.50 cm. It supports the collection of 50,000 echoes, the magnetic field strength is 0.28 ± 0.03 T, the detection is 1H nuclei, the uniformity of the magnet in the detection area is higher than 30 ppm, the frequency source ranges from 1 to 30 MHz, and the frequency control accuracy reaches 0.1 Hz. The $T_2$ spectrum was obtained using the CPMG pulse sequence and SIRT inversion algorithm. The NMR analyzer is produced by Suzhou Niumag Analytical Instrument Co., Ltd., Suzhou, China. The NM-V type vacuum pressurization and saturation device has a maximum withstand pressure of 50 MPa, a working pressure varying from 0 to 40 MPa, and a core sample chamber volume of 1500 mL, manufactured by Suzhou Niumag Analytical Instrument Co., Ltd., Suzhou, China. The volume of the ZR-3 type piston intermediate container is 250 mL, and the working pressure is in the range of 0 to 70 MPa. The pump volume of the high-pressure pump is 200 mL, with a pressure range of 0 to 50 MPa. The temperature control range of the constant temperature heating device is between −20 and 280 °C.

In this experiment, a high-pressure soaking test was performed to simulate the effect of fracturing fluid damage. The optimal time for core soaking was usually determined by the variation of macroscopic parameter permeability. This study proposes a method for determining the optimal time for shale high-pressure soaking based on NMR, which truly reflects the effect of fracturing fluid on the microscopic pore volume and greatly shortens the test time. That is, shale NMR $T_2$ spectrum tests of high-pressure soaking for different times (0 h, 48 h, and 72 h) were completed, respectively (Figure 1). The curve of the NMR $T_2$ spectrum gradually decreases with the increase in soaking time. The reducing amplitude of the NMR $T_2$ spectrum curve indicates the reduction value of pore volume from fracturing fluid damage. When the difference between the decrease in shale $T_2$ spectrum curve measured after soaking for 48 h and 72 h is less than 0.50%, the optimal soaking time is 48 h.

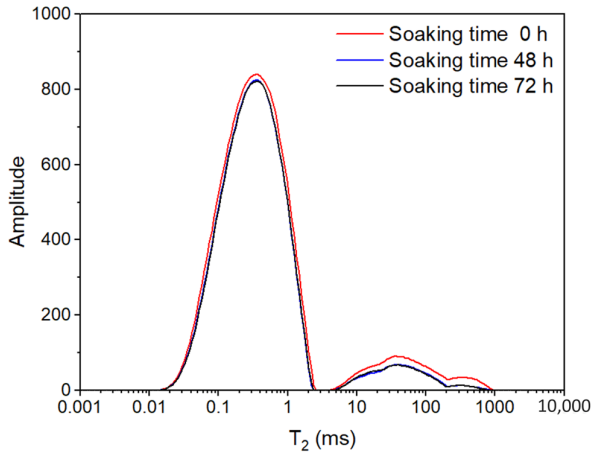


**Figure 1.** NMR $T_2$ spectrum of shale under different soaking times.

The experimental schematic diagram is shown in Figure 2. The experimental procedures are as follows:

(1) Shale cores with a diameter of 2.50 cm and a length of 6.00 cm were drilled using an anhydrous wire-cutting machine. The length of 6.00 cm core plungers (A1-2, A2-2, B1-2, B2-2) were cut from the core face, and then used in shale high-pressure soaking tests (Figure 3). The permeability of the core was tested using nitrogen gas and calculated.

(2) After the shale cores were evacuated by a vacuum pressurization and saturation device for 6 h, the formation water was saturated with high pressure for 24 h. Core porosity was calculated by weighing, and the core's NMR $T_2$ spectrum test was executed. Subsequently, the core was dried at 100 °C for 24 h in a drying oven.

(3) Under the formation temperature of 65 °C, the dry core was placed in an intermediate container filled with fracturing fluid, soaking at a formation pressure of 20 MPa for 48 h, and then, the core was dried at 100 °C for 24 h.
(4) Repeating step (2), the permeability of the core was tested using nitrogen and calculated.

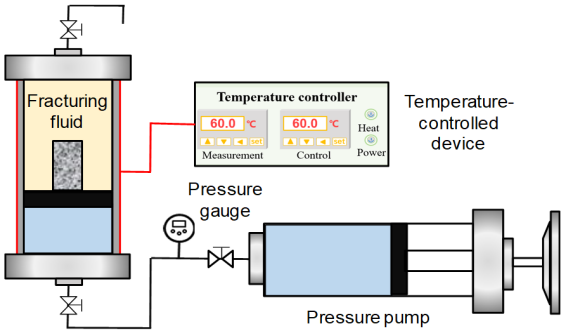


**Figure 2.** Schematic diagram of shale high-pressure soaking test.

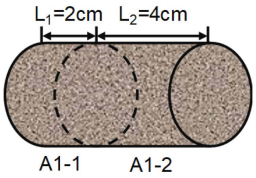


**Figure 3.** Schematic diagram of core cutting.

### *2.3. Shale Mineral Composition Test*

For the shale mineral composition test, the SmartLab X-ray diffractometer was utilized, which is manufactured by Japan Rigaku Corporation, Osaka, Japan. It has a horizontal goniometer with a minimum step of 1/10,000 degrees. The CBO cross-optical path provides a focusing optical path and a high-intensity and high-resolution parallel optical path. The high-speed detector D/teX-Ultra250 is used, and its energy resolution is less than 20%. According to the Petroleum and Natural Gas Industry Standard SY/T5163-2018 "X-ray Diffraction Analysis Method for Clay Minerals and Common Non-clay Minerals in Sedimentary Rocks", the remaining 2.00 cm length cores (A1-1, A2-1, B1-1, B2-1) and the cores (A1-2, A2-2, B1-2, B2-2) after soaking were selected, which were crushed and ground until all particle sizes were less than 40 μm. The test pieces were made and loaded onto the sample table of the SmartLab X-ray diffractometer, obtaining the characteristic diffraction peak intensities of minerals. The content of whole rock minerals and clay minerals were determined using SmartLab Guidance intelligent measurement and analysis software. The quantitative analyses of the difference in shale mineral content and its effect on the microscopic pore structure were conducted.

### *2.4. Test of Iron Ion Concentration in Fracturing Fluid*

An UV-2600 type spectrophotometer with double beams was selected, whose wavelength is between 185 and 900 nm, the wavelength accuracy is ±0.10 nm, and manufactured by Japan Shimadzu Corporation, Kyoto, Japan. Before and after the high-pressure soaking test, 10 mL of the filtrate were taken, respectively, from the $EM30^+$ + guar gum mixed water and CNI nano variable-viscosity slickwater. Based on the coal industry standard of the People's Republic of China MT/T368-2005 "Determination of iron ions in coal mine water", for the fracturing fluid, the phenanthroline colorimetric method was used to determine the discrepancy in concentrations of ferrous ions, ferric ions, and total iron ions.

### 2.5. Experimental Evaluation Method

According to the shale porosity, permeability, and saturated formation water NMR $T_2$ spectrum before and after the high-pressure soaking test by the fracturing fluid, the calculated equations of pore-throat damage degree, porosity damage degree, and permeability damage degree of the shale are given in Equations (1)–(3), respectively. The pore-throat damage degree is utilized to calculate the pore damage ratio as Equation (4).

$$I_{pti} = \frac{A_{bi} - A_{ai}}{A_{bi}} \times 100\% \quad (1)$$

$$I_{\phi} = \frac{\phi_b - \phi_a}{\phi_b} \times 100\% \quad (2)$$

$$I_K = \frac{K_b - K_a}{K_b} \times 100\% \quad (3)$$

$$R_{pti} = \frac{I_{pti}}{\sum_{i=1}^{3} I_{pti}} \times 100\% \quad (4)$$

where $I_{pti}$ is the pore-throat damage degree of a certain pore type, %, $A_{bi}$ is the overlying area of the saturated formation water NMR $T_2$ spectrum of a certain pore type, that is, the total signal of the NMR $T_2$ spectrum before the high-pressure soaking test, ms, $A_{ai}$ is the overlying area of the saturated formation water NMR $T_2$ spectrum of a certain pore type, that is, the total signal of the NMR $T_2$ spectrum after the high-pressure soaking test, ms, $I_{\phi}$ is the porosity damage degree of the core, %, $\phi_b$ is the core porosity before high-pressure soaking test, %, $\phi_a$ is the core porosity after high-pressure soaking test, %, $I_K$ is the permeability damage degree of the core, %, $K_b$ is the gas measured permeability of the core before high-pressure soaking test, $10^{-3}$ μm$^2$, $K_a$ is the gas measured permeability of the core after high-pressure soaking test, $10^{-3}$ μm$^2$, and $R_{pti}$ is the ratio of the pore-throat damage degree of a certain pore type to the total pore-throat damage degree of the shale core, %.

## 3. Results

### 3.1. The Influence on Pore Volume

To enhance the comparability of the measurement results of different cores, the amplitude of NMR $T_2$ spectrum was normalized for shales saturated with the formation water before and after high-pressure soaking experiments (Figure 4). The difference in the $T_2$ value reflects the distinct pore size, and the amplitude value (amplitude normalized value) indicates the corresponding amount of pores with various pore apertures. The NMR $T_2$ spectrum curve of shale saturated with the formation water exhibit three peaks (Figure 4). Based on the former research results [45], the subregion $T_2$ values corresponding to the troughs of the curves were determined and averaged by the $T_2$ spectral curves of the saturated water in the four cores. The shale's pore types are divided into micropore (<2.29 ms), mesopore (2.29 to 48.49 ms), and macropore/microfracture (>48.49 ms). The shale's pore types are dominated by micropores, followed by mesopores, and lastly macropores, with the highest content of micropores.

The amplitude curve of the NMR $T_2$ spectrum of the core saturated with formation water declined after immersion (Figure 4), and the total pore volume decreased by 0.63%–5.62% (pore-throat damage degree). The pore volume diminished, and the pore structure inflicted a certain degree of fracturing fluid damage. The curve areas of the $T_2$ spectra of different pore types also presented a decline with different degrees. The decreased ranges of micropores, mesopores, and macropores are 0.02%–5.88%, 3.13%–5.93%, and 0.47%–7.24%, respectively. The results demonstrated that there were differences in damage to the shale's microscopic pore structure, which was caused by types of fracturing

fluids and drag reducer concentrations. While the NMR curve after soaking displayed a small increase locally, that is, the pore volume corresponding to the $T_2$ spectrum increased.

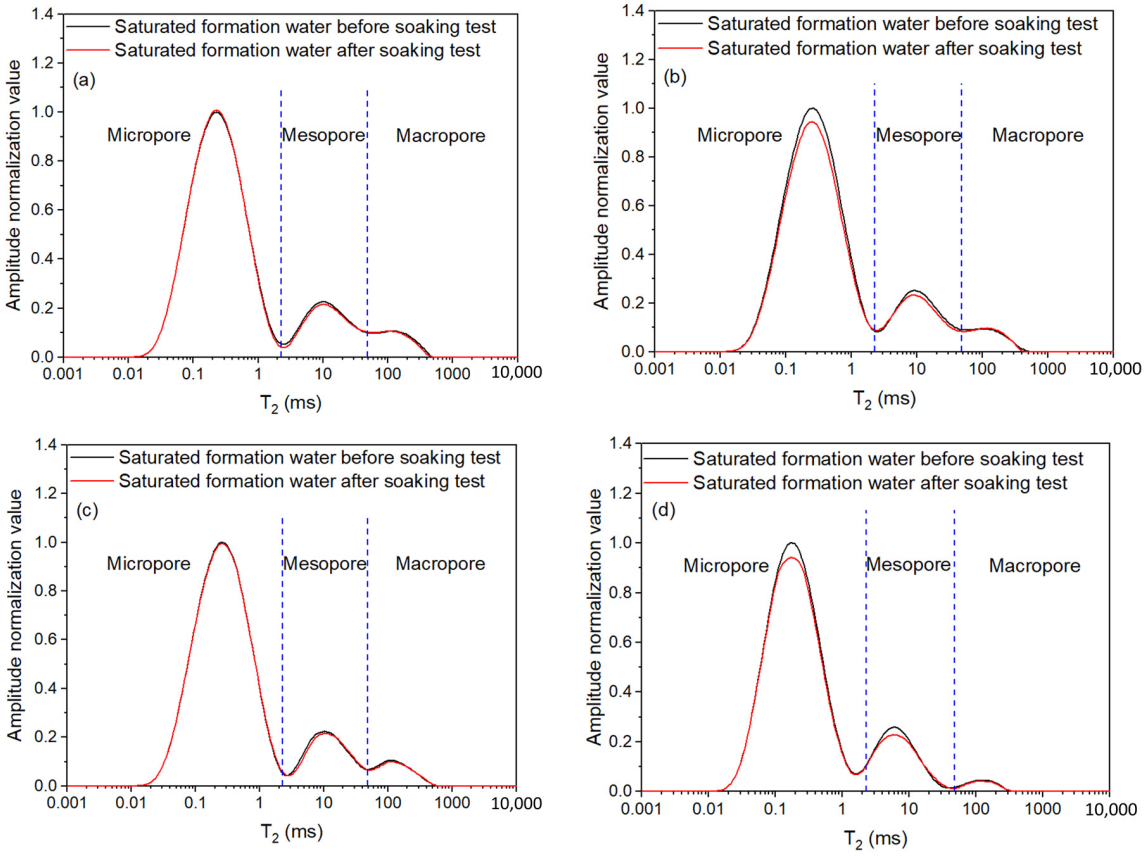


**Figure 4.** NMR $T_2$ distribution curves of shales saturated with formation water before and after the high-pressure soaking test: (**a**) core A1-2; (**b**) core A2-2; (**c**) core B1-2; (**d**) core B2-2.

Figure 5 shows a comparison of the damage ratio of different pore types in the core. The mesopores of the A1-2 and B1-2 cores were mainly damaged by the fracturing fluid, followed by the marcopores, and there was little damage to the micropores. For A2-2 and B2-2 cores, the pore type of the main damage is micropores, followed by mesopores, and the least damage to macropores.

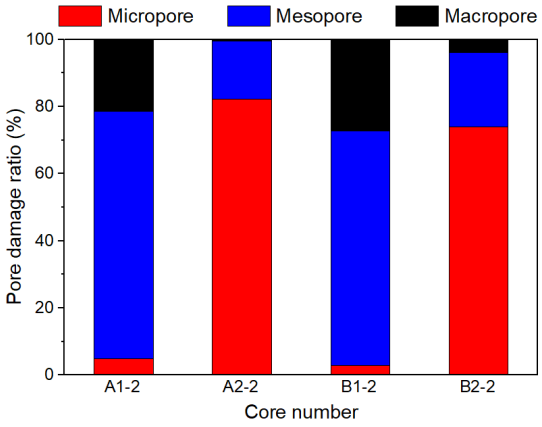


**Figure 5.** Pore damage ratio of different pore types in shale.

### *3.2. The Influence on Porosity and Permeability*

The invasion of fracturing fluid into the shale led to different reductions in the porosity and permeability. The porosity damage degree and permeability damage degree ranged from 1.51 to 6.84% and 4.17 to 19.61%, respectively. The permeability damage degree is higher than the porosity damage degree and the pore-throat damage degree. As the pore-throat damage degree of shales intensified, the porosity damage degree increased slowly, whereas the permeability damage degree escalated sharply (Figure 6). The fracturing fluid is less harmful to the shale pore, but its permeability is greatly reduced, which makes it more difficult for the subsequent injection or production fluid to flow into the shale.

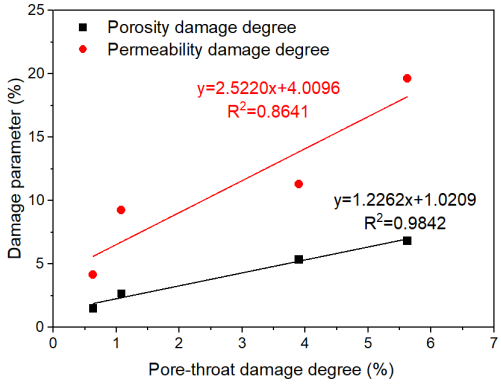


**Figure 6.** The relationship between damage parameters (porosity damage degree and permeability damage degree) and pore-throat damage degree.

### *3.3. The Influence on Shale Mineral Composition*

According to Figure 7a,b, shale minerals mainly include quartz and clay minerals, a small amount of feldspar and carbonate minerals, and a very small amount of iron-bearing minerals, such as pyrite and siderite. The content of shale minerals featured various changes after soaking. The content of feldspar and iron-bearing minerals increased by 3.70 to 18.10% and 0.50 to 2.70%, respectively. The content of carbonate minerals and clay minerals lessened by 0.20 to 5.50% and 1.20% to 9.40%, respectively. Nevertheless, the obvious disparity occurred in the variation regularity of quartz content. For instance, the quartz content after soaking in EM30$^+$ + guar gum mixed water reduced in the range of 0.80 to 3.70%, and the quartz content soaked in CNI nano variable-viscosity slickwater had an increase of 0.90% to 1.90%. The addition in content of illite was from 1.00 to 9.00%, the reduction in content of mixed-layer illite/smectite was from 2.00 to 8.00%, and the kaolinite content decreased to zero.

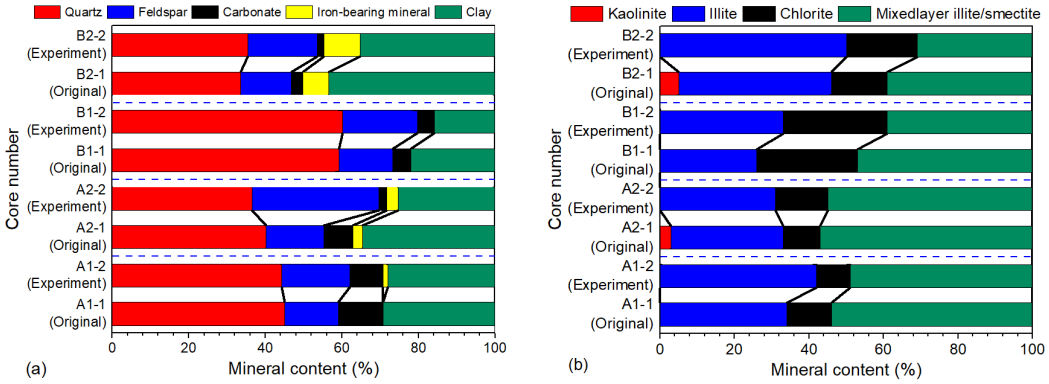


**Figure 7.** Shale minerals content before and after the high-pressure soaking test: (**a**) whole-rock minerals; (**b**) clay minerals.

### *3.4. The Influence on Iron Ion Concentration of the Fracturing Fluid*

The variation in iron ion concentration of the fracturing fluid were compared before and after the soaking test (Figure 8). The concentrations of ferrous ions and total iron ions were reduced by 0.07 to 2.59 mg/L and 0.07 to 1.13 mg/L, respectively. However, the concentrations of ferric ions were increased by 1.19 to 1.69 mg/L in CNI nano variable-viscosity slickwater.

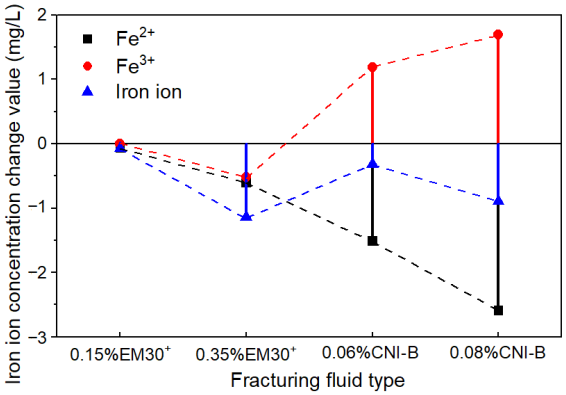


**Figure 8.** Changes in iron ion concentration in the fracturing fluid.

## 4. Discussion

### *4.1. Effect of Fracturing Fluid Types*

The NMR $T_2$ spectrum curves of the four shales saturated with formation water are similar in shape. Furthermore, there is basically no discrepancy in the content of micropores, mesopores, and macropores, porosity, and permeability. Therefore, the influence of the shale physical properties and pore structure on the results of fracturing fluid high-pressure soaking tests was disregarded. The 0.35% $EM30^+$ + guar gum mixed water had the highest damage degree of the shale pore throat, followed by 0.08% CNI-B nano variable-viscosity slickwater and 0.15% $EM30^+$ + guar gum mixed water, and the smallest was the 0.06% CNI-B nano variable-viscosity slickwater. The damage of $EM30^+$ + guar gum mixed water on the shale is higher than that of the CNI nano variable-viscosity slickwater (Figure 6). The main reason is that guar gum molecules have the characteristics of heightened adsorption and retention on the rock surface. Moreover, $EM30^+$ + guar gum mixed water is an alkaline solution, thereby enhancing the reaction of silicate minerals. As a result, the stability of minerals deteriorated, underpinning the formation damage. Consequently, the shale suffered less damage from CNI nano viscous slickwater fracturing fluid. With the increase in the concentration of $EM30^+$ or CNI-B drag reducer, the effect of the drag reduction increased, improving the injection performance of the fracturing fluid. More fracturing fluid molecules entered the micropores to increase the degree of damage on the micropores. Additionally, the amount of adsorption on the rock surface grew in number, further intensifying the pore-throat damage degree (Figure 5).

### *4.2. Effect of Mineral Composition*

In addition to the types and properties of fracturing fluid, the physical and chemical interactions between fracturing fluid and shale are directly dominated by the types and compositions of minerals, which in turn, detrimentally affect the microscopic pore structure, porosity, and permeability. Therefore, the relationship between shale mineral content and porosity damage degree, permeability damage degree, and pore throat damage was analyzed (Figures 9 and 10).

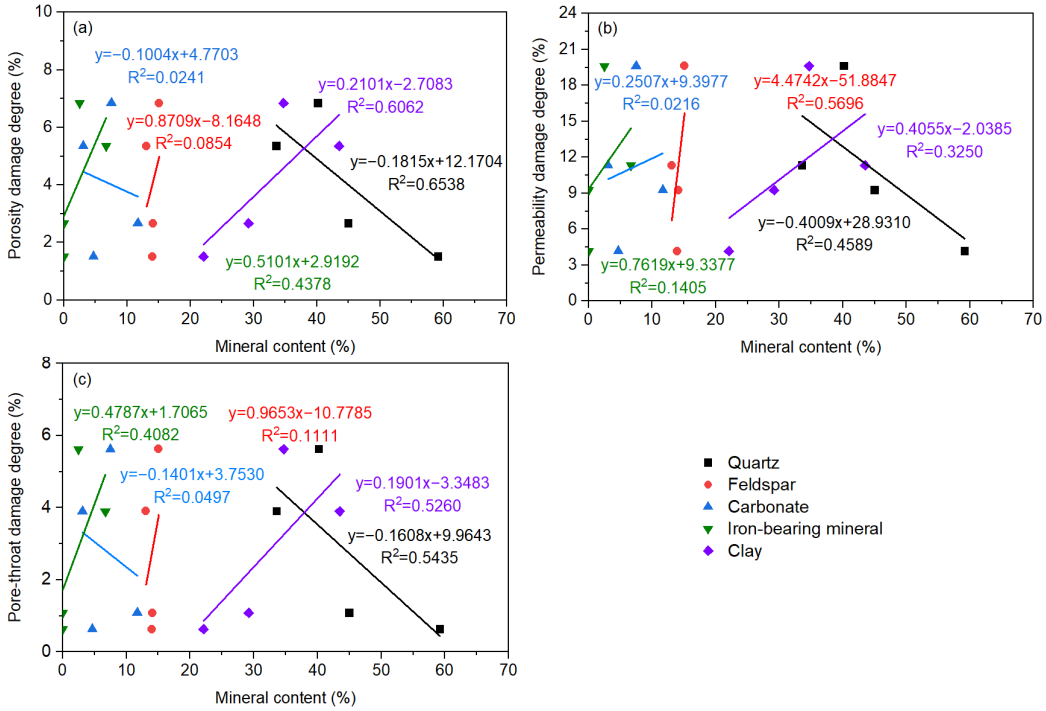


**Figure 9.** The relationship between damage parameters and shale whole-rock minerals: (**a**) porosity damage degree; (**b**) permeability damage degree; (**c**) pore-throat damage degree.

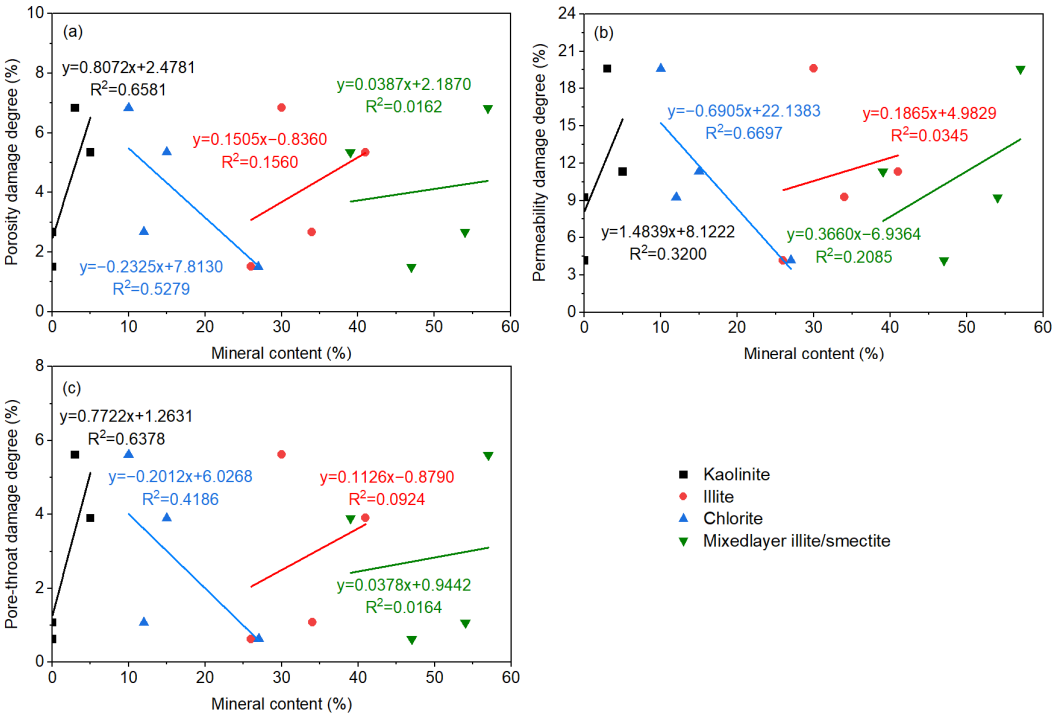


**Figure 10.** The relationship between damage parameters and shale clay minerals: (**a**) porosity damage degree; (**b**) permeability damage degree; (**c**) pore-throat damage degree.

The porosity damage degree, permeability damage degree, and pore-throat damage degree are highly negatively correlated with quartz, while they are positively correlated with clay minerals and iron-bearing minerals. The damage of shale with a low content of quartz and high content of clay minerals and iron minerals was amplified. The degree of chemical reaction of quartz is relatively low, and in comparison, the interactions between

the clay minerals, iron-bearing minerals, and fracturing fluid are enhanced. Compared with the porosity damage degree and the pore-throat damage degree, the correlation between the permeability damage degree and the above mineral composition is significantly lower, indicating that the mineral types and compositions have a more complex effect on the permeability damage. The positive correlation between permeability damage degree and feldspar is also high. That is, the higher the feldspar content, the greater the shale permeability damage degree. From neutral to alkaline fracturing fluid, minerals (feldspar and clay) undergo different degrees of reactions, thereby increasing the content of feldspar and decreasing the content of clay minerals. Additionally, the dissolution of quartz in alkaline $EM30^+$ + guar gum mixed water increased, with a lessening in the quartz content. Dissolved shale formed new carbonate mineral precipitation (dolomite forming calcite and soluble carbonate after alkaline dissolution) and iron-bearing mineral precipitation, which led to a reduction in the content of carbonate minerals and an increment in the iron-bearing mineral content (Figure 7a).

The porosity damage degree, permeability damage degree, and pore-throat damage degree are highly correlated with kaolinite and chlorite. They are positively correlated with kaolinite and negatively correlated with chlorite. As the kaolinite content is higher or the chlorite content is lower, the harmfulness to shale augments. A strong positive correlation was also found between the permeability damage degree and mixed-layer illite/smectite. The hydration was inflicted on the highly hydration-swellable mixed-layer illite/smectite, causing a sharp reduction in the radius of micropores and throats, and a rapid decline in the core permeability. After soaking, the content of kaolinite and mixed-layer illite/smectite curtailed, indicating the occurrence of mineral dissolution, accompanied by the formation of secondary silicate and other minerals. In addition, the chlorite was dissolved to form dissolution pores and illite, increasing the content of illite (Figure 7b). Meanwhile, the mineral particles on the rock surface flaked off and migrated, resulting in the deterioration of the microscopic pore structure. This conclusion is consistent with the research viewpoints of Hakala et al. [46] and Herz-Thyhsen et al. [47].

### *4.3. Effect of Iron Ion Concentration*

There are two main reasons for the variations in the concentration of ferrous ions, ferric ions, and total iron ions in fracturing fluid. Firstly, iron ions formed iron-containing minerals and their precipitates with anions, such as $CO_3^{2-}$ and $OH^-$, that is, iron ions came from fracturing fluid or were released by dissolving minerals, such as pyrite and siderite. Secondly, under neutral and alkaline conditions, ferrous ions are less stable and easily converted into ferric ions and iron hydroxide precipitates, which reduced the concentration of ferrous ions (Figure 8) and underpinned the content of iron-containing minerals (Figure 7a). Tan et al. also proposed that mineral dissolution in neutral and alkaline fracturing fluids will release more iron ions, followed by the formation of new precipitates, which is consistent with the experimental results of this study [48].

Figure 11 shows the relationship between the variation values of total iron ion concentration in the fracturing fluid and damage parameters. As the concentration of total iron ion diminished, the pore-throat damage degree and porosity damage degree gradually augmented, and the permeability damage degree showed a rapid increment. The main reason for the above phenomenon is that iron ions generated precipitated iron, reducing the pore spaces and blocking the throats. Therefore, the formation damage caused by the iron ion or iron-containing minerals was not neglected. Iron ion stabilizers could inhibit the precipitation of iron precipitates and effectively reduce the damage of fracturing fluids on shale formations, which illustrated the necessity of adding iron ion stabilizers into fracturing fluids.

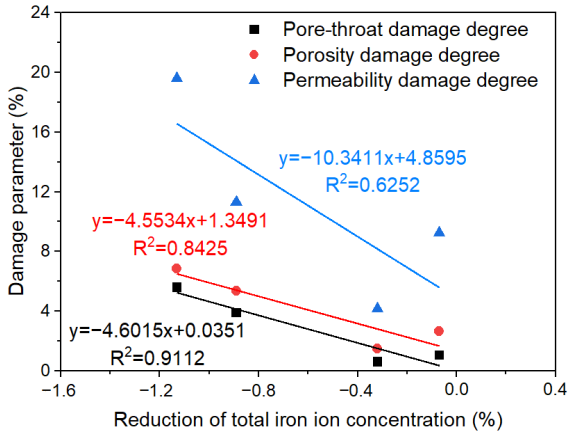


**Figure 11.** The relationship of damage parameters with total iron ion concentration in fracturing fluid.

### *4.4. Mechanism of Damage to Shale Pore Structure*

In contrast with CNI nano variable-viscosity slickwater, the larger molecular diameter of $EM30^{+}$ + guar gum mixed water has a higher retention. When the fracturing fluid invaded into the shale, silicate minerals, carbonate minerals, and iron-containing minerals underwent dissolution reactions, which increased the pore volume and new flow channels and improved the microscopic pore structure. Nevertheless, the secondary mineral precipitates and exfoliated particles deteriorated the pore-throat connectivity and then damaged the pore structure. In particular, shale characterized by a high content of iron minerals and clay minerals (silicate minerals) is more harmful to the microscopic pore structure. The water-sensitivity montmorillonite produced obvious hydration expansion in the mixed-layer illite/smectite, and the corresponding pore volume decreases sharply. These effects led to variations in the shale pore volume, increased surface roughness, and severe throat blockage. The small damage on the shale pores caused a large decrease in the core permeability, which fully explained the results of the shale high-pressure soaking test (Figure 12).

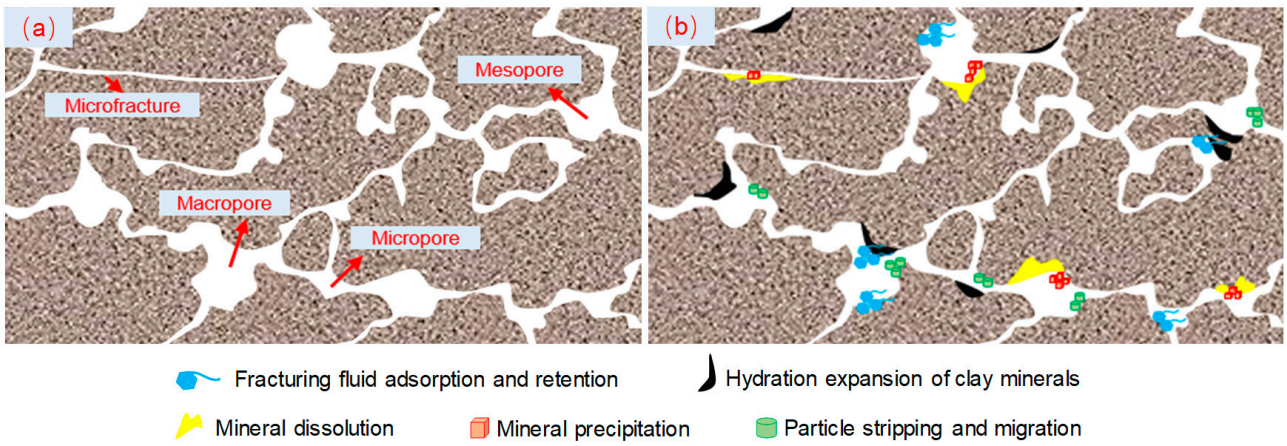


**Figure 12.** Schematic diagram of damage mechanism of shale's microscopic pore structure: (**a**) original shale; (**b**) shale after high-pressure soaking.

## 5. Conclusions

The high-pressure soaking tests of shale in the fracturing fluid were launched with NMR technology, and the damage degree of different scale pores of shale was quantitatively characterized. The macroscopic physical properties (porosity, permeability) and damage characteristics of pore types at different scales of shale were quantitatively characterized. The effects of the fracturing fluid type, mineral composition, and iron ion concentration on

the microscopic pore structure of shale were analyzed in depth. Finally, the microscopic damage mechanism of shale was revealed.

1. The invasion of fracturing fluid caused the reduction of shale pore volume. The permeability damage degree is higher than that of the porosity damage degree and pore throat damage degree. $EM30^+$ + guar gum mixed water is more harmful to shale than CNI nano variable-viscosity slickwater. Moreover, with the increase in concentrations of $EM30^+$ and CNI-B, the shale pore damaged by fracturing fluid gradually transitions from macropore and mesopore to micropore.
2. The lower content of quartz, higher content of clay minerals and iron-bearing minerals in shale would enhance the mineral dissolution and precipitation degree, leading to serious damage of the pore structure. Moreover, iron ions in the fracturing fluid and iron-bearing minerals react chemically to generate iron precipitates. The damage on the microscopic pore structure was intensified. So, the addition of iron ion stabilizers into fracturing fluids is proposed to reduce the damage of shale formations.
3. $EM30^+$ + guar gum mixed water fracturing fluid is highly deleterious to shale; the main reason is that the drastic effects of fracturing fluid adsorption retention, mineral dissolution, and precipitation. In addition, the damage mechanisms also include the hydration expansion of the mixed-layer illite/smectite, the migration of mineral particles and the sediments.

**Author Contributions:** Conceptualization, Z.W.; methodology, Y.Y. and Z.W.; validation, N.Z.; data curation, X.Z.; visualization, X.Z.; formal analysis, X.Z.; investigation, X.Z. and T.L.; resources, C.Z.; writing—original draft preparation, X.Z.; writing—review and editing, T.L. and Z.C.; supervision, H.G., T.L. and C.W.; project administration, H.G. All authors have read and agreed to the published version of the manuscript.

**Funding:** This research was funded by the National Natural Science Foundation of China (Grant Nos. 52174030 and 52204044), the Postgraduate Innovation and Practice Ability Development Fund of Xi'an Shiyou University (Grant No. YCS21211013), Key Research and Development Program of Shaanxi Province (Grant Nos. 2022GY-137 and 2022JQ-528), Key Scientific Research Project of Education Department of Shaanxi Province (Grant No. 21JP095), Petro-China Innovation Foundation (Grant No. 2020D-5007-0205), the Open Fund of State Key Laboratory of Petroleum Resources and Prospecting, China University of Petroleum, (PRP/open-2214), Science and Technology Planning Project of Gansu Province (Grant No. 23YFGM0001), and funded by Open Foundation of Shaanxi Key Laboratory of Lacustrine Shale Gas Accumulation and Exploitation, and the Youth Innovation Team of Shaanxi Universities.

**Data Availability Statement:** Not applicable.

**Conflicts of Interest:** The authors declare no conflict of interest.

## References

1. Babatunde, K.A.; Negash, B.M.; Jufar, S.R.; Ahmed, T.Y.; Mojid, M.R. Adsorption of gases on heterogeneous shale surfaces: A review. *J. Pet. Sci. Eng.* **2022**, *208*, 109466. [CrossRef]
2. Xu, Y.; Lun, Z.; Pan, Z.; Wang, H.; Zhou, X.; Zhao, C.; Zhang, D. Occurrence space and state of shale oil: A review. *J. Pet. Sci. Eng.* **2022**, *211*, 110183. [CrossRef]
3. Niu, W.; Lu, J.; Sun, Y.; Liu, H.; Cao, X.; Zhan, H.; Zhang, J. A review of the application of data-driven technology in shale gas production evaluation. *Energy Rep.* **2023**, *10*, 213–227. [CrossRef]
4. Guo, R.; Li, S.; Zhou, X.; Guo, Q.; Li, S.; Chen, J.; Zhang, J.; Hao, L.; Ma, X.; Qiu, J.; et al. Multi-Isothermal Stage Pyrolysis of the Chang $7_3$ Shale Oil Reservoirs, Ordos Basin: Implications for Oil Occurrence States and In Situ Conversion Exploitation. *ACS Earth Space Chem.* **2022**, *6*, 1143–1162. [CrossRef]
5. Seales, M.B. Multiphase Flow in Highly Fractured Shale Gas Reservoirs: Review of Fundamental Concepts for Numerical Simulation. *ASME J. Energy Resour. Technol.* **2020**, *142*, 100801. [CrossRef]
6. Clarkson, C.R.; Haghshenas, B.; Ghanizadeh, A.; Qanbari, F.; Williams-Kovacs, J.D.; Riazi, N.; Debuhr, C.; Deglint, H.J. Nanopores to megafractures: Current challenges and methods for shale gas reservoir and hydraulic fracture characterization. *J. Nat. Gas Sci. Eng.* **2016**, *31*, 612–657. [CrossRef]
7. Mojid, M.R.; Negash, B.M.; Abdulelah, H.; Jufar, S.R.; Adewumi, B.K. A state-of-art review on waterless gas shale fracturing technologies. *J. Pet. Sci. Eng.* **2021**, *196*, 108048. [CrossRef]

8. Feng, Y.; Xiao, X.; Wang, E.; Gao, P.; Lu, C.; Li, G. Gas storage in shale pore system: A review of the mechanism, control and assessment. *Pet. Sci.* 2023. [CrossRef]
9. Harrison, A.L.; Jew, A.D.; Dustin, M.K.; Thomas, D.L.; Joe-Wong, C.M.; Bargar, J.R.; Johnson, N.; Brown, G.E.; Maher, K. Element release and reaction-induced porosity alteration during shale-hydraulic fracturing fluid interactions. *Appl. Geochem.* **2017**, *82*, 47–62. [CrossRef]
10. She, J.; Zhang, H.; Zhong, Y.; Yuan, Y.; You, J. Alkali Solution Erodes Shale: Influencing Factors and Structural Damage Characteristics. *J. Chem.* **2018**, *2018*, 3641627. [CrossRef]
11. Zhang, W.; Zhang, D.; Zhao, J. Experimental investigation of water sensitivity effects on microscale mechanical behavior of shale. *Int. J. Rock Mech. Min. Sci.* **2021**, *145*, 104837. [CrossRef]
12. Lyu, Q.; Shi, J.; Tan, J.; Dick, J.M.; Kang, X. Effects of shale swelling and water-blocking on shale permeability. *J. Pet. Sci. Eng.* **2022**, *212*, 110276. [CrossRef]
13. Lei, Q.; Xu, Y.; Cai, B.; Guan, B.; Wang, X.; Bi, G.; Li, H.; Li, S.; Ding, B.; Fu, H.; et al. Progress and prospects of horizontal well fracturing technology for shale oil and gas reservoirs. *Pet. Explor. Dev.* **2022**, *49*, 191–199. [CrossRef]
14. Medina-Rodriguez, B.X.; Frouté, L.; Alvarado, V.; Kovscek, A.R. Multimodal study of the impact of stimulation pH on shale pore structure, with an emphasis on organics behavior in alkaline environments. *Fuel* **2023**, *331*, 125649. [CrossRef]
15. Lyu, Q.; Shi, J.; Pathegama Gamage, R. Effects of testing method, lithology and fluid-rock interactions on shale permeability: A review of laboratory measurements. *J. Nat. Gas Sci. Eng.* **2020**, *78*, 103302. [CrossRef]
16. Yan, Q.; Lemanski, C.; Karpyn, Z.T.; Ayala, L.F. Experimental investigation of shale gas production impairment due to fracturing fluid migration during shut-in time. *J. Nat. Gas Sci. Eng.* **2015**, *24*, 99–105. [CrossRef]
17. Xu, Z.; Li, Z.; Wang, C.; Adenutsi, C.D. Experimental study on microscopic formation damage of low permeability reservoir caused by HPG fracturing fluid. *J. Nat. Gas Sci. Eng.* **2016**, *36*, 486–495. [CrossRef]
18. You, L.; Zhou, Y.; Kang, Y.; Yang, B.; Cui, Z.; Cheng, Q. Fracturing fluid retention in shale gas reservoirs:mechanisms and functions. *Arab J Geosci.* **2019**, *12*, 779. [CrossRef]
19. Zhang, L.; Zhou, F.; Zhang, S.; Li, Z.; Wang, J.; Wang, Y. Evaluation of permeability damage caused by drilling and fracturing fluids in tight low permeability sandstone reservoirs. *J. Pet. Sci. Eng.* **2019**, *175*, 1122–1135.
20. Khan, H.J.; Spielman-Sun, E.; Jew, A.D.; Bargar, J.; Kovscek, A.; Druhan, J.L. A Critical Review of the Physicochemical Impacts of Water Chemistry on Shale in Hydraulic Fracturing Systems. *Environ. Sci. Technol.* **2021**, *55*, 1377–1394. [CrossRef]
21. Wu, Y.; Cheng, L.; Ma, L.; Huang, S.; Fang, S.; Killough, J.; Jia, P.; Wang, S. A transient two-phase flow model for production prediction of tight gas wells with fracturing fluid-induced formation damage. *J. Pet. Sci. Eng.* **2021**, *199*, 108351. [CrossRef]
22. Xu, C.; Kang, Y.; You, Z.; Chen, M. Review on formation damage mechanisms and processes in shale gas reservoir: Known and to be known. *J. Nat. Gas Sci. Eng.* **2016**, *36*, 1208–1219. [CrossRef]
23. Sun, Z.; Wang, Y.; Wei, Z.; Ni, Y.; Wu, B.; Li, J.; Fan, W.; Wang, G.; Li, Y. Pore Structure Alteration Characteristics of Different Mineralogical Composition Shale during Shale-Fracturing Fluid Physical-Chemical Interactions. *Geofluids* **2019**, *2019*, 5047643. [CrossRef]
24. Zhang, Y.; Li, Z.; Lai, F.; Wu, H.; Mao, G.; Adenutsi, C.D. Experimental Investigation into the Effects of Fracturing Fluid-Shale Interaction on Pore Structure and Wettability. *Geofluids* **2021**, *2021*, 6637955. [CrossRef]
25. Liu, K.; Wang, D.; Sheng, J.J.; Li, J. Review of the Generation of Fractures and Change of Permeability due to Water-Shale Interaction in Shales. *Geofluids* **2022**, *2022*, 1748605. [CrossRef]
26. Bazin, B.; Bekri, S.; Vizika, O.; Herzhaft, B.; Aubry, E. Fracturing in Tight Gas Reservoirs: Application of Special-Core-Analysis Methods to Investigate Formation-Damage Mechanisms. *SPE J.* **2010**, *15*, 969–976. [CrossRef]
27. Tariq, Z.; Kamal, M.S.; Mahmoud, M.; Shakil Hussain, S.M.; Hussaini, S.R. Novel gemini surfactant as a clay stabilizing additive in fracturing fluids for unconventional tight sandstones: Mechanism and performance. *J. Pet. Sci. Eng.* **2020**, *195*, 107917. [CrossRef]
28. Tariq, Z.; Kamal, M.S.; Mahmoud, M.; Murtaza, M.; Abdulraheem, A.; Zhou, X. Dicationic Surfactants as an Additive in Fracturing Fluids to Mitigate Clay Swelling: A Petrophysical and Rock Mechanical Assessment. *ACS Omega* **2021**, *6*, 15867–15877. [CrossRef]
29. Ahmed Khan, R.; Murtaza, M.; Abdulraheem, A.; Kamal, M.S.; Mahmoud, M. Imidazolium-Based Ionic Liquids as Clay Swelling Inhibitors: Mechanism, Performance Evaluation, and Effect of Different Anions. *ACS Omega* **2020**, *5*, 26682–26696. [CrossRef]
30. Li, Y.; Wang, S.; Guo, J.; Chen, R.; Zhao, F.; Liu, Y. Reducing adsorption of hydroxypropyl guar gum on sandstone by silicon nanoparticles. *Carbohydr. Polym.* **2019**, *219*, 21–28. [CrossRef]
31. Jew, A.D.; Dustin, M.K.; Harrison, A.L.; Joe-Wong, C.M.; Thomas, D.L.; Maher, K.; Brown, G.E., Jr.; Bargar, J.R. Impact of Organics and Carbonates on the Oxidation and Precipitation of Iron during Hydraulic Fracturing of Shale. *Energy Fuels* **2017**, *31*, 3643–3658. [CrossRef]
32. Edgin, M.G.; Medina-Rodriguez, B.; Kaszuba, J.P.; Dewey, J.C.; Alvarado, V. Geochemical reactions and alteration of pore architecture in saturated shale after injection of stimulation fluid. *Fuel* **2021**, *303*, 120815. [CrossRef]
33. Hu, C.; Tan, J.; Lyu, Q.; Feng, G.; Shi, J.; Wang, K.; Wang, Z. Variations of shale's pore characteristics and hydraulic properties after long-term imbibition in hydraulic fracturing fluids. *Geomech. Geophys. Geo-Energy Geo-Resour.* **2022**, *8*, 183. [CrossRef]
34. Jew, A.D.; Druhan, J.L.; Ihme, M.; Kovscek, A.R.; Battiato, I.; Kaszuba, J.P.; Bargar, J.R.; Brown, G.E., Jr. Chemical and Reactive Transport Processes Associated with Hydraulic Fracturing of Unconventional Oil/Gas Shales. *Chem. Rev.* **2022**, *122*, 9198–9263. [CrossRef]

35. Lu, Y.; Liu, J.; Tang, J.; Ao, X.; Li, H.; Zhou, J.; Sun, X. Pore changes of slickwater-containing shale under supercritical $CO_2$ treatment. *Fuel* **2022**, *312*, 122775. [CrossRef]
36. Qi, A.; Qian, P.; Huang, H.; Ren, D.; Gu, X.; Zhang, F.; Yuan, X. Research on the Characteristics of Microscopic Damage to Different Pore Types by Slippery Water Fracturing Fluid in the Chang Member Tight Sandstone Reservoir, Ordos Basin, NW China. *Geofluids* **2021**, *2021*, 6652877. [CrossRef]
37. Zhang, K.; Liu, Y.; Sheng, L.; Li, B.; Chen, T.; Liu, X.; Yao, E. Study on the Effect of Fracturing Fluid on the Structure and Mechanical Properties of Igneous Rock. *ACS Omega* **2022**, *7*, 11903–11913. [CrossRef]
38. Sun, Z.; Ni, Y.; Wang, Y.; Wei, Z.; Wu, B.; Li, J.; Fan, W.; Wang, G.; Li, Y. Experimental investigation of the effects of different types of fracturing fluids on the pore structure characteristics of Shale Reservoir Rocks. *Energy Explor. Exploit.* **2020**, *38*, 682–702. [CrossRef]
39. Cheng, B.; Li, J.; Li, J.; Su, H.; Tang, L.; Yu, F.; Jiang, H. Pore-scale formation damage caused by fracturing fluids in low-permeability sandy conglomerate reservoirs. *J. Pet. Sci. Eng.* **2022**, *208*, 109301. [CrossRef]
40. Hua, G.; Wu, S.; Jing, Z.; Yu, X.; Xu, K.; Shi, W.; Guan, M. Rock physical and chemical alterations during the in-situ interaction between fracturing fluid and Silurian organic-rich shales in China. *J. Nat. Gas Sci. Eng.* **2021**, *94*, 104075. [CrossRef]
41. Li, X.; Zhang, Q.; Liu, P.; Li, T.; Liu, G.; Liu, Z.; Zhao, H. Investigation on the microscopic damage mechanism of fracturing fluids to low-permeability sandstone oil reservoir by nuclear magnetic resonance. *J. Pet. Sci. Eng.* **2022**, *209*, 109821. [CrossRef]
42. Guo, T.; Gong, F.; Lin, X.; Lin, Q.; Wang, X. Experimental Investigation on Damage Mechanism of Guar Gum Fracturing Fluid to Low-Permeability Reservoir Based on Nuclear Magnetic Resonance. *ASME J. Energy Resour. Technol.* **2018**, *140*, 072906. [CrossRef]
43. Li, Y.; Jiang, G.; Li, X.; Yang, L. Quantitative Investigation of Water Sensitivity and Water Locking Damages on a Low-Permeability Reservoir Using the Core Flooding Experiment and NMR Test. *ACS Omega* **2022**, *7*, 4444–4456. [CrossRef] [PubMed]
44. Guo, J.; Li, Y.; Wang, S. Adsorption damage and control measures of slick-water fracturing fluid in shale reservoirs. *Pet. Explor. Dev.* **2018**, *45*, 336–342. [CrossRef]
45. Wei, B.; Zhang, X.; Liu, J.; Xu, X.; Pu, W.; Bai, M. Adsorptive behaviors of supercritical $CO_2$ in tight porous media and triggered chemical reactions with rock minerals during $CO_2$-EOR and -sequestration. *Chem. Eng. J.* **2020**, *381*, 122577. [CrossRef]
46. Hakala, J.A.; Paukert Vankeuren, A.N.; Scheuermann, P.P.; Lopano, C.; Guthrie, G.D. Predicting the potential for mineral scale precipitation in unconventional reservoirs due to fluid-rock and fluid mixing geochemical reactions. *Fuel* **2021**, *284*, 118883. [CrossRef]
47. Herz-Thyhsen, R.J.; Kaszuba, J.P.; Dewey, J.C. Mineral dissolution and precipitation induced by hydraulic fracturing of a mudstone and a tight sandstone in the Powder River Basin, Wyoming, USA. *Appl. Geochem.* **2020**, *119*, 104636. [CrossRef]
48. Tan, J.; Hu, C.; Lyu, Q.; Feng, G.; Chen, S. Experimental investigation on the effects of different fracturing fluids on shale surface morphology. *J. Pet. Sci. Eng.* **2022**, *212*, 110356. [CrossRef]